FEW-LAYER $MoTe_2$ SUSPENDED CHANNEL TRANSISTORS AND NANOELECTROMECHANICAL RESONATORS

Xia Liu, Arnob Islam, Philip X.-L. Feng
Department of Electrical Engineering & Computer Science, Case School of Engineering, Case Western Reserve University, 10900 Euclid Avenue, Cleveland, OH 44106, USA

ABSTRACT

Molybdenum ditelluride ($MoTe_2$) is a rapidly emerging two-dimensional (2D) transition metal dichalcogenide (TMDC) layered material thanks to the features of low energy barrier for phase transition and the sizeable bandgap close to that of silicon (Si). These attractive features make it a focus of substantial research interest in future nanoelectronics. Here, we report on the first demonstration of few-layer $MoTe_2$ suspended channel transistors (SCTs) and nanoelectromechanical resonators operating in the high frequency (HF) regime. $MoTe_2$ SCTs exhibit *On/Off* ratio levels at $I_{On}/I_{Off} \approx 10^4$. We also present the passivation of $MoTe_2$ resonators by using hexagonal boron nitride (h-BN) crystal, which essentially creates h-BN/$MoTe_2$ heterostructure bimorphs. Moreover, we investigate the electrical tuning of the resonator and observe resonance frequency tuning of $\Delta f/f \approx 13\%$ by varying gate voltage (V_G) from 0 to -16V.

KEYWORDS

Nanoelectromechanical systems (NEMS), resonator, 2D materials, $MoTe_2$, suspended channel transistor, optical interferometry, frequency tuning.

INTRODUCTION

Actuating and sensing nanoscale vibration are challenging and important in realizing new tools for exploring ultrasmall objects and machines of interest. Nanoelectromechanical systems (NEMS) based on atomically thin crystals, such as graphene [1,2], transition metal dichalcogenides (TMDCs) [3,4,5]. These two-dimensional (2D) crystals feature ultralow mass and superior mechanical flexibility. TMDCs, as a rising class of 2D materials beyond graphene, have attracted intense attention from different research fields in boosting 2D nanoelectronics [6]. TMDCs are especially suitable for new transistors by virtue of their sizeable bandgaps compatible with those of conventional semiconductors. Moreover, these semiconducting TMDCs show reliable transition from indirect to direct bandgap when scaled down to the single-layer limit [7,8,9]. They also offer different *crystal structures* and *phases* so that they may be accessed and configured to achieve programmable functions. Recently, a new member of the TMDC family, molybdenum ditelluride ($MoTe_2$), is receiving increasing attention due to its unusual semiconducting, metallic, and superconducting properties [10, 11, 12]. Single-layer $MoTe_2$ is theoretically predicted and experimentally demonstrated to have the bandgap of 1.1 eV [13], which excellently matches the bandgap of silicon (Si). These features make it an important focus of substantial research interest in explorations for future nanoelectronics, *e.g.*, field-effect transistors (FETs), phase change memory, *etc.* In theory, the acoustic phonon-limited electron mobility of $MoTe_2$ is over 2,500 $cm^2V^{-1}s^{-1}$ (14). In contrast to MoS_2, $MoTe_2$ mainly shows p-type (or p-dominated ambipolar) behavior when prepared by using flux of tellurium.

In addition to its exceptional electrical properties, 2D $MoTe_2$ has lower strain limit for phase transition ($\varepsilon \sim 1.5\%$) [8] and elastic modulus ($E_Y \sim 88$ to 112 GPa in 2H phase) [15]. These combined properties suggest intriguing possibilities for innovating nanoscale electromechanical transducers where the mechanical properties of 2D $MoTe_2$ are coupled to its band structure and other electronic and optoelectronic attributes (unavailable in graphene). However, nanoscale electromechanically coupled $MoTe_2$ devices have not yet been explored.

In this work, we first demonstrate the experimental results of electromechanical coupling effects in $MoTe_2$ SCT and resonator as illustrated in Figure 1. Figure 1a presents an illustration of the h-BN encapsulated $MoTe_2$ (h-BN/$MoTe_2$) FET on 290 nm-thick silicon oxide (SiO_2) with heavily p-doped Si as the global back gate. In order to increase the stability of the transistor performance, we transfer thin h-BN flake on top of $MoTe_2$, so that the chemically active Te atoms on the surface are prevented from exposure to ambient environment. The h-BN encapsulated $MoTe_2$ transistors behave as pristine p-type FETs. Figure 1b illustrates the electromechanical transduction mechanism of the $MoTe_2$ suspended channel transistor and resonator. The electrostatic force induced by the gate voltage modulates the strain of the channel and leads to a resonance frequency shift of the resonator.

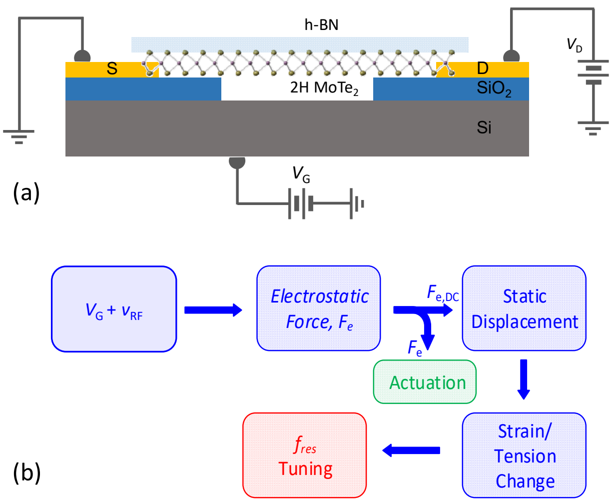

Figure. 1: $MoTe_2$ suspended channel transistor (SCT) and resonator. (a) Illustration of the cross-section of $MoTe_2$ SCT and resonator. (b) Block diagram explaining the resonance frequency tuning (or called electromechanical coupling) of $MoTe_2$ SCT and resonantor via modulating the strain by gate voltage (V_G).

DEVICE DESIGN AND FABRICATION

In this study, we fabricate $MoTe_2$ SCTs or resonators by using a dry-transfer method. We classify two categories of suspended $MoTe_2$ SCTs: one is bare $MoTe_2$ and the other one is with the encapsulation by h-BN. Au is selected as the electrode material due to the moderate work function ($\emptyset_m$ = 4.8 eV) compared with other metals (such as Pt, Ni and Ti), so the Fermi level is at around the midgap of the $MoTe_2$ semiconductor [16]. Figure 2 shows the fabrication procedure of the $MoTe_2$ SCT and resonator. First, the microtrench is fabricated on the SiO_2/Si substrate using photolithography. Then the electrodes are fabricated and patterned onto a Si wafer covered with the 290 nm-thick thermal oxide (SiO_2) using photolithography and metal deposition. The substrates with source/drain (S/D) electrodes are cleaned in acetone and isopropyl alcohol (IPA) using a sonicator, and dried using a N_2 gun. Next, a $MoTe_2$ flake with uniform thickness is transferred onto the SiO_2/Si substrate. During the transfer, it is necessary to keep 2–4° anchor between the flake and the substrate in order not to trap bubbles in the interface between the $MoTe_2$ layer and the substrate. For the h-BN encapsulated transistors, the second transfer step is conducted by exfoliating the h-BN flake from h-BN bulk crystal (HQ graphene). The shape of the h-BN flake is carefully chosen in order to fully encapsulate the $MoTe_2$ flake.

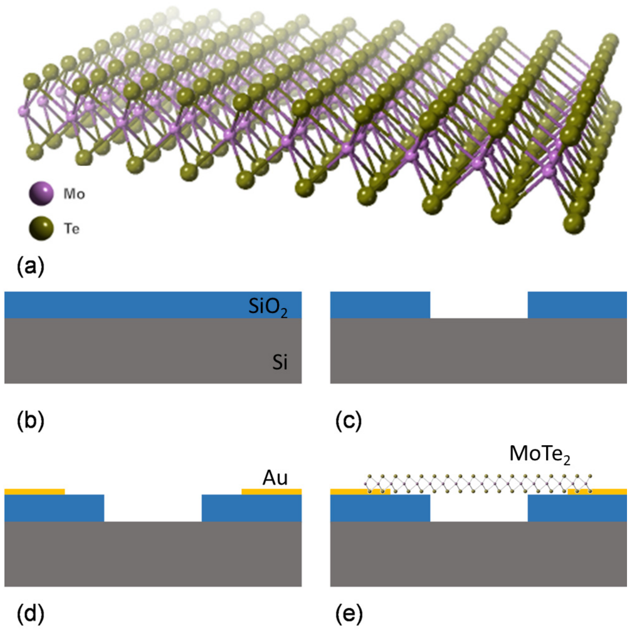

Figure 2: (a) 3D crystal structure of 2H $MoTe_2$. (b) Fabrication starts with a bare 290nm SiO_2 on Si substrate. (c) 1st photolithography step for making microtrenches. (d) 2nd photolithography step: deposit metal (40nm Au/5nm Cr) to create electrodes and metal contact pads. (e) Finally few-layer $MoTe_2$ is transferred on top of pre-patterned electrodes and microtrenches to fabricate $MoTe_2$ SCTs.

Figure 3a shows the cross-section of a $MoTe_2$ SCT. In order to fabricate $MoTe_2$ SCT, a $MoTe_2$ flake is dry transferred across the pre-patterned source and drain gold (Au) electrodes, fully covering a microtrench (Fig. 3b). The other $MoTe_2$ SCT presented in Fig. 3c shows that the $MoTe_2$ flake is fully covered by the h-BN flake. Figure 3d shows an optical microscopy image of the h-BN encapsulated $MoTe_2$ device. The distinctive colors of the flakes indicate the stacking layers of the h-BN/$MoTe_2$ heterostructure. h-BN is used to prevent $MoTe_2$ from ambient degradation. At first, we investigate the transistor or DC characteristics of the $MoTe_2$ SCT. Later, we detect the resonance frequency by using optical interferometric readout with electrostatic actuation using the global back gate. Figure 4 shows that Raman spectroscopy probing (λ = 532 nm) on the h-BN/$MoTe_2$ stack of the back-gate FET provides us with the overall information about the identities of the constitutive flakes [17]. The characteristic Raman-active modes of A_{1g} (171 cm^{-1}), E^1_{2g} (233 cm^{-1}), and B^1_{2g} (292 cm^{-1}) are clearly observed, demonstrating the high quality of $MoTe_2$ after the transfer process. The h-BN encapsulation layer is also identified by Raman.

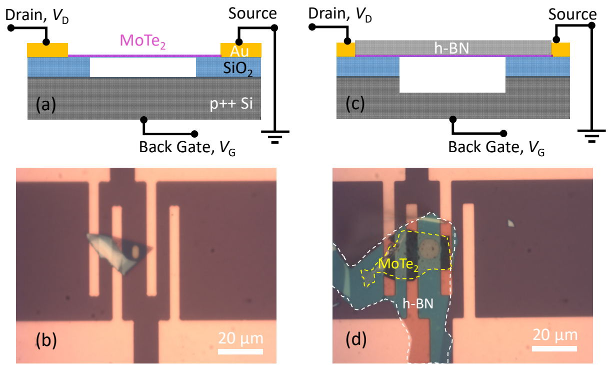

Figure 3: (a) Schematic of the device without h-BN encapsulation. (b) Optical microscopy image of the $MoTe_2$ suspended channel transistor (SCT). (c) Schematic of the h-BN encapsulated $MoTe_2$ device. (d) Optical microscopy image of the device, in which the h-BN flake (white dashed line enclosure) completely encapsulates the $MoTe_2$ flake (yellow dashed line enclosure).

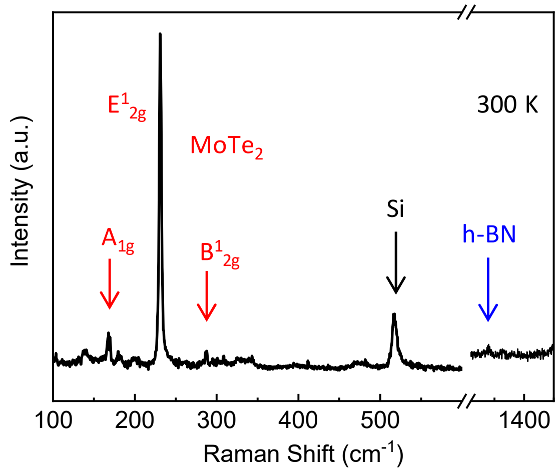

Figure 4: Raman spectroscopy data obtained from h-BN encapsulated $MoTe_2$ SCT and resonator.

RESULTS AND DISCUSSIONS

We present the gate voltage and drain voltage sweeping characteristics of $MoTe_2$ SCT in Fig. 5. Figure 5a shows the transfer characteristic, the drain-to-source current (I_D) as a function of V_G for the uncovered $MoTe_2$ transistor. As observed from the data, the transistor behaves as unipolar p-type with $I_{On}/I_{Off} > 10^4$. Figure 5b shows that I_D as a function of V_D decreases with increasing V_G, indicating p-type conduction. As seen, the linear I_D–V_D characteristic indicates narrow and low Schottky barrier and the hole carriers can tunnel through it. With the encapsulation, the $MoTe_2$ transistor displays improved transistor performance in terms of higher On-State current (Fig. 5c & 5d).

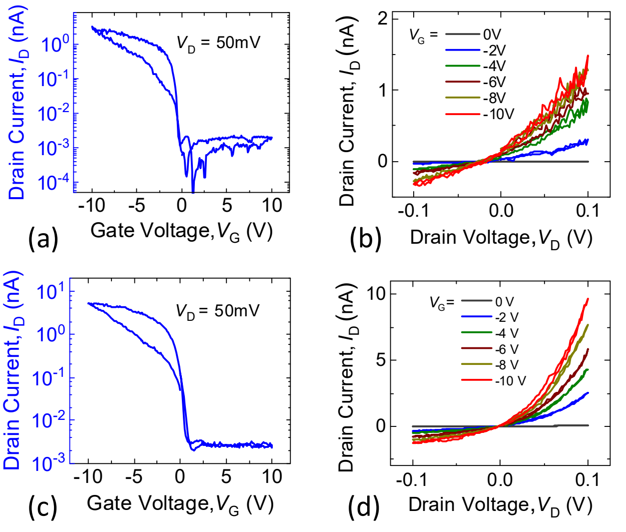

Figure 5: Electrical characteristics and performance of the $MoTe_2$ SCTs. Uncovered $MoTe_2$ SCT: (a) I_D (in a logarithmic scale) as a function of the gate voltage, V_G. (b) I_D versus V_D, with several values of the back-gate voltage. h-BN encapsulated $MoTe_2$ SCT: (c) I_D (in a logarithmic scale) as a function of the gate voltage, V_G. (d) I_D versus V_D, with several values of the back-gate voltage.

After that, we measure the resonance of the device using the established optical interferometry in conjunction with electrostatic actuation by the global back gate. The electrostatic actuation and simultaneous optical detection of resonance frequency (f_{res}) is shown in Fig. 6a. A He-Ne laser (633 nm) with spot size of ~1 µm is used for optical interferometric readout [3,3,18]. For $MoTe_2$ resonator, we obtain the fundamental resonance mode, f_{res} = 9.15 MHz with quality (Q) factor ~ 264 as shown in Fig. 6b. Figure 7a shows the resonance frequencies of an h-BN encapsulated $MoTe_2$ SCT tuned by changing V_G. The resonance frequency of the first mode (~11.5 MHz) increases with $|V_G|$; so does that of the second mode (~18 MHz). We observe frequency tuning, $\Delta f/f \approx 13\%$ by varying $|V_G|$ from 0 to 16V (Fig. 7b). Higher V_G induces static deflection due to electrostatic force. This deflection causes tensile strain in the $MoTe_2$ suspended channel, which translates into tensile stress. This tensile stress causes upshift or hardening of the resonance frequency. The frequency tuning range depends on the initial strain in the resonator and 2D Young's modulus of the material. Figure 7c shows change of Q values with gate tuning. Q factor decreases at higher V_G due to loaded-Q effect [19]. Figure 8 shows the measured resonance frequency with increasing RF excitation strength (v_{RF}). It shows the increase of the resonance peak amplitude with increasing v_{RF}.

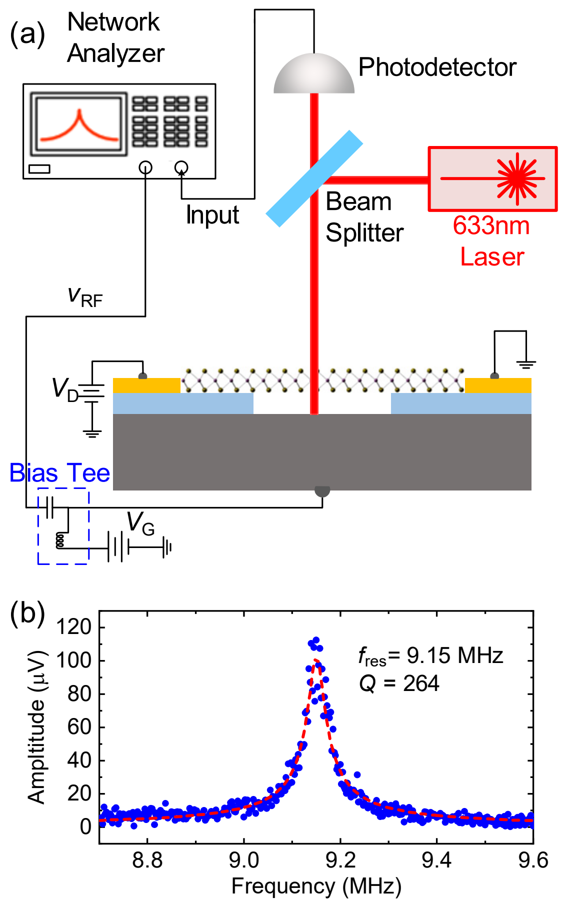

Figure 6: Optical interferometric measurement of the few-layer $MoTe_2$ NEMS resonator. (a) Detection of resonance frequency of $MoTe_2$ resonator by using sensitive laser interferometry and back-gate electrostatic excitation. (b) Optically measured resonance of a $MoTe_2$ resonator.

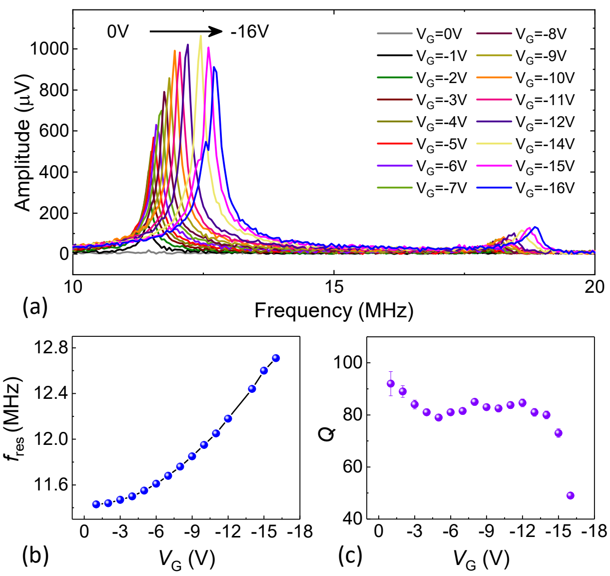

Figure 7: (a) Gate tuning of resonance frequencies of the h-BN encapsulated $MoTe_2$ vibrating channel transistor at fixed RF driving amplitude (V_{RF} = 50mV). (b) Resonance frequency (f_{res}) with varying DC gate voltage. (c) Quality (Q) factor with varying DC gate voltage.

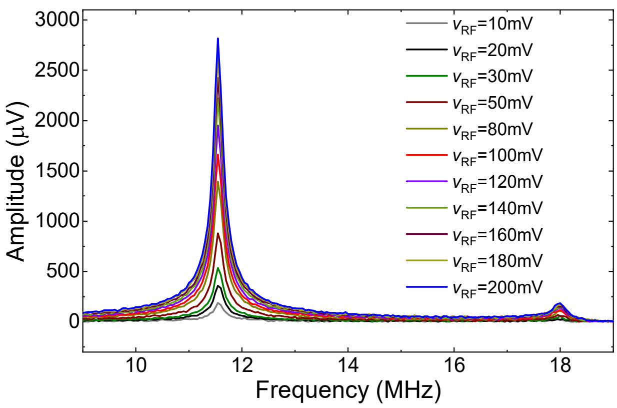

Figure 8: Measurement of resonance frequencies of the h-BN encapsulated $MoTe_2$ SCT under various excitation strength with sweeping RF driving amplitude and at fixed DC gate voltage (V_G=-5V).

CONCLUSION

In summary, in this paper we have described the first demonstration of $MoTe_2$ suspended channel transistors and resonators, which can be explored in future for resonant sensing applications and signal processing functions. The electromechanical frequency tuning of $\Delta f/f \approx 13\%$ is observed by varying back-gate voltage V_G from 0 to -16V. In addition, $MoTe_2$ transistors encapsulated by thin h-BN crystal have excellent stability thanks to the passivation effect of h-BN, manifesting the potential utility of h-BN encapsulation for fabricating suspended channel transistors and NEMS resonators incorporating other environmentally susceptible semiconductors. The semiconducting nature of $MoTe_2$ will enable all-electrical readout of the resonances (*e.g.*, via vibrating channel transistor scheme), for future on-chip integration by utilizing the SCT platform.

ACKNOWLEGEMENTS

We thank financial support from the National Science Foundation (NSF) through an EPMD Award (Grant #ECCS-1810154) and CAREER Award (Grant #ECCS-1454570), and the Wen H. Ko Fellowship. We also thank X.-Q. Zheng, H. Jia, and Y. Wang for technical support and helpful discussions.

REFERENCES

[1] J. S. Bunch, *et al.*, "Electromechanical Resonators from Graphene Sheets", *Science*, vol. 315, pp. 490–493, 2007.

[2] F. Ye, J. Lee, P. X.-L. Feng, "Electrothermally Tunable Graphene Resonators Operating at Very High Temperature up to 1200 K", *Nano Letters*, vol. 18, pp. 1678–1685, 2018.

[3] J. Lee, Z. Wang, K. He, J. Shan; P. X.-L. Feng, "High Frequency MoS_2 Nanomechanical Resonators", *ACS Nano*, vol. 7, pp. 6086–6091, 2014.

[4] K. Deng, *et al.*, "Experimental Observation of Topological Fermi Arcs in Type-II Weyl Semimetal $MoTe_2$", *Nature Phys.*, vol. 12, pp. 1105–1110, 2016.

[5] Y. Li, *et al.*, "Measurement of the Optical Dielectric Function of Monolayer Transition Metal Dichalcogenides: MoS_2, $MoSe_2$, WS_2, and WSe_2", *Phys. Rev. B*, vol. 90, art. no. 205422, 2014.

[6] M. Chhowalla, *et al.*, "The Chemistry of Two-Dimensional Layered Transition Metal dichalcogenide Nanosheets", *Nature Chem.*, vol. 5, pp. 263–275, 2013.

[7] G. R. Bhimanapati, *et al.*, "Recent Advances in Two-Dimensional Materials beyond Graphene", *ACS Nano*, vol. 9, pp. 11509–11539, 2015.

[8] K. N. Duerloo, Y. Li, E. J. Reed, "Structural Phase Transitions in Two-Dimensional Mo- and W-Dichalcogenide Monolayers", *Nature Commun.*, vol. 5, art. no. 4214, 2014.

[9] D. H. Keum, *et al.*, "Bandgap Opening in Few-Layered Monoclinic $MoTe_2$", *Nature Phys.*, vol. 11, pp. 482–486, 2015.

[10] A. Roy, *et al.*, "Structural and Electrical Properties of $MoTe_2$ and $MoSe_2$ Grown by Molecular Beam Epitaxy", *ACS Appl. Mater. Interfaces*, vol. 8, pp. 7396–7402, 2016.

[11] Y. Qi, *et al.*, "Superconductivity in Weyl Semimetal Candidate $MoTe_2$", *Nature Commun.*, vol. 7, art. no. 11038, 2016.

[12] K. S. Novoselov, A. Mishchenko, A. Carvalho, A. H. Castro Neto, "2D Materials and van der Waals Heterostructures", *Science*, vol 353, aac9439, 2016.

[13] J. Yang, *et al.,* "Robust Excitons and Trions in Monolayer $MoTe_2$", *ACS Nano*, vol. 9, pp. 6603–6609, 2015.

[14] J.-H. Huang, *et al.,* "Large-Area 2D Layered $MoTe_2$ by Physical Vapor Deposition and Solid-Phase Crystallization in a Tellurium-Free Atmosphere", *Adv. Mater. Interfaces*, vol. 4, art. no. 1700157, 2017.

[15] Y. Sun, *et al.*, "Elastic Properties and Fracture Behaviors of Biaxially Deformed, Polymorphic $MoTe_2$", *Nano Letters*, vol. 19, pp. 761−769, 2019.

[16] S. Nakaharai, M. Yamamoto, K. Ueno, K. Tsukagoshi, "Carrier Polarity Control in α-$MoTe_2$ Schottky Junctions Based on Weak Fermi-Level Pinning", *ACS Appl. Mater. Interfaces*, vol. 8, pp. 14732–14739, 2016.

[17] C. Ruppert, O. B. Aslan, T. F. Heinz, "Optical Properties and Band Gap of Single- and Few-layer $MoTe_2$ Crystals", *Nano Letters*, vol. 14, pp. 6231–6236, 2014.

[18] Z. Wang, J. Lee, P. X.-L. Feng, "Spatial Mapping of Multimode Brownian Motions in High-Frequency Silicon Carbide Microdisk Resonators", *Nature Commun.*, vol. 5, art. no. 5158, 2014.

[19] J. Lee, Z. Wang, K. He, R. Yang, J. Shan, P. X.-L. Feng, "Electrically Tunable Single- and Few-Layer MoS_2 Nanoelectromechanical Systems with Broad Dynamic Range", *Science Advances*, vol. 4, art. no eaao6653, 2018.

CONTACT

Xia Liu: xia.liu4@case.edu
Arnob Islam: arnob.islam@case.edu
Philip X.-L. Feng: philip.feng@case.edu